Title

Optimization for Axial Resolution, Depth Range, and Sensitivity of Spectral Domain Optical Coherence Tomography at 1.3 μm.

Journal

Journal of the Korean Physical Society, 55(6)

ISSN

0374-4884

Authors

Lee, Sang-Won

Jeong, Hyun-Woo

Kim, Beop-Min

et al.

Publication Date

2009-12-15

DOI

10.3938/jkps.55.2354

Published in final edited form as:
J Korean Phys Soc. 2009 December 12; 55(6): 2354–2360. doi:10.3938/jkps.55.2354.

Optimization for Axial Resolution, Depth Range, and Sensitivity of Spectral Domain Optical Coherence Tomography at 1.3 μm

Sang-Won Lee,
Research Institute of Health Sciences, Korea University, Seoul 136-703 and Department of Biomedical Engineering, Korea University, Seoul 136-703

Hyun-Woo Jeong,
Department of Biomedical Engineering, Korea University, Seoul 136-703

Beop-Min Kim[*],
Department of Biomedical Engineering, Korea University, Seoul 136-703

Yeh-Chan Ahn,
Beckman Laser Institute and Department of Biomedical Engineering, University of California, Irvine, Irvine, CA 92697, U.S.A.

Woonggyu Jung[†], and
Beckman Laser Institute and Department of Biomedical Engineering, University of California, Irvine, Irvine, CA 92697, U.S.A.

Zhongping Chen[‡]
Beckman Laser Institute and Department of Biomedical Engineering, University of California, Irvine, Irvine, CA 92697, U.S.A.

Abstract

We have developed high-speed and high-resolution spectral domain optical coherence tomography at 1.3 μm using an InGaAs line-scan camera and a broadband light source with the bandwidth of 170 nm that produces a theoretical axial resolution of 4.4 μm in air. We compared axial resolutions from point spread functions (PSFs) and depth ranges while changing the full spectral bandwidth detected by the camera and describing the optimization process for the axial resolution, the depth range, and the sensitivity for SD-OCT system. We found that SD-OCT at 1.3 μm cannot satisfy the conditions both below the axial resolution of 5 μm and above the depth range of 2 mm because of the restricted pixel number of the line-scan camera. To scan a large depth range, the axial resolution has to be sacrificed. In addition, the sensitivity rolls off slowly as a function of the depth if a large depth range is scanned. On the other hand, if the axial resolution needs to be close to the theoretical one, the depth range becomes limited and the sensitivity decays quickly. Since we have to maintain a reasonable depth range of 2.0 mm, we chose the spectrum full bandwidth of 214 nm captured by the detector to balance the axial resolution of 8.2 μm. In this setting, the sensitivity of our OCT system was measured at 107.1 dB. Theoretical and experimental results are compared and presented in this paper.

Keywords

Spectral domain optical coherence tomography; Axial resolution; Depth range; Sensitivity

[*]Corresponding author 1: bmk515@korea.ac.kr; Tel: +82-2-940-2883; Fax: +82-2-941-2883. [‡]Corresponding author 2: c2chen@uci.edu; Tel: +1-949-824-1247; Fax: +1-949-824-8413.
[†]Currently: Beckman Institute for Advanced Science and Technology, University of Illinois at Urbana-Champaign, Urbana, IL 61801, U.S.A.

I. INTRODUCTION

Optical coherence tomography (OCT), a high-resolution imaging technology, has been developed and popularly used to obtain cross-sectional and functional images of the internal microstructure of biological tissues *in vivo* [1–4]. The high axial resolution below 10 μm makes it possible to obtain in-vivo tomographic images close to the level of histology. The axial resolution of OCT is inversely proportional to the optical bandwidth of the low coherent light source [5,6]. Ophthalmic and endoscopic OCT can produce 1 ~ 3 μm resolution images using a light source with a full width half maximum (FWHM) well above 100 nm such as an ultrashort pulse laser, which is coupled with a long optical fiber to provide dispersive stretching of the pulse duration, or a superluminescence diode (SLD) combined with several SLD modules [7–11].

High acquisition speed is needed for real-time imaging and 3-D volume rendering without motion artifacts especially when *in-vivo* imaging for living biological samples is necessary [12,13]. In conventional time-domain OCT (TD-OCT), interference signals are measured as a function of time while the reference arm is scanned [5,6,14]. The axial scan rates of TD-OCT are limited to several kilohertz due to mechanical movement and insufficient sensitivity [14,15].

Recently, Fourier-domain OCT (FD-OCT) based on either a spectrometer (spectral-domain OCT, SD-OCT) or a frequency-swept laser source (swept-source OCT, SS-OCT or optical frequency domain imaging, OFDI) has been actively studied. FD-OCT detects spectrally resolved interference signals, which are generated by the optical path length difference between the reference mirror and the sample [12, 13, 15]. FD-OCT requires no depth scanning, and the acquisition speed is limited by the read-out rate of the line-scan camera or the sweeping-rate of the laser [16–18]. Real-time imaging is easily enabled because the data acquisition time in FD-OCT is much shorter. In addition, it has been reported that the sensitivity of FD-OCT is theoretically 24 ~ 27 dB higher than that of TD-OCT [17].

SD-OCT at 800-nm regions with an ultrahigh resolution, a high speed, and a large scan depth range has been developed using a high-power, large-bandwidth light source and line-scan charge-coupled-devices (CCD) or a complementary metal-oxide semiconductor (CMOS) camera with large pixel numbers (over 1024 pixels). A high acquisition speed (above 20 klines/s) can be achieved at relatively low cost [7–9]. Until recently, the SD-OCT at 1.3 μm has not been actively studied because the commercially available InGaAs line-scan cameras had small pixel numbers and slow acquisition speed at high cost [12,13,19,20]. In addition, the light source at 1.3 μm with FWHM bandwidth above 100 nm used to be quite costly. Recently, a high-speed InGaAs line-scan camera was commercialized; it has 1024 pixels and an acquisition rate of higher than 40 klines/s. Further, a moderately priced broadband and high-powered SLD with a bandwidth of more than 150 nm at 1310 nm has become available.

In this paper, we constructed an SD-OCT with these high-speed InGaAs line-scan camera and broadband SLD. Additionally, we compared axial resolutions from point spread functions (PSFs) and depth ranges while changing the full spectral bandwidth detected by the camera and describing the optimization process for the axial resolution, the depth range, and the sensitivity of our SD-OCT system. We found that the axial resolution had to be somehow sacrificed to maintain a scan depth range of more than 2 mm. Actual images of biological tissues were compared based on these parameters.

II. PRINCIPLES

An axial resolution is an important specification of an OCT system. The axial resolution, half of the coherence length (lc), can be defined by the center wavelength (λ_0) and the full width half maximum (FWHM, $\Delta\lambda$) of the optical source as follows [5,6]:

$$\Delta z = \frac{2\ln 2}{\pi}\frac{\lambda_0^2}{\Delta\lambda}, \quad (1)$$

The depth range (z_{max}) is limited by the wavenumber spacing between pixels (δk) of the spectrometer. The depth range in the Fourier domain is given by [16]

$$z_{max} = \frac{\pi}{2\delta k} \text{ and } \delta k = \frac{2\pi\lambda_{full}}{N\lambda_0^2}, \quad (2)$$

where λ_{full} and N are the full spectral bandwidth and the total pixel number of the line-scan camera, respectively. The interval (δz) between image pixels in the axial direction of an OCT image can be determined as the depth range divided by half of the total pixel number (N/2). From Eq. (2), we can represent the δz as follows:

$$\delta z = \frac{\lambda_0^2}{2\lambda_{full}}, \quad (3)$$

The δz should be smaller than half the theoretical axial resolution from Eq. (1) to satisfy the Nyquist sampling theorem [8]. Therefore, the full spectral bandwidth detected by the spectrometer should satisty [8]

$$\lambda_{full} \geq \frac{\pi}{2(\ln 2)}\Delta\lambda = 2.26618\Delta\lambda \quad (4)$$

Fig. 1 shows the relationships between the theoretically calculated axial resolution based on the FWHM of the light source (red) and twice the z value calculated from Eq. (3) with the full spectral bandwidth at 840 nm (a) and 1310 nm (b) regions, respectively. To obtain the same δz at 840 nm, the full spectral bandwidth at 1310 nm has to be broader than that at 840 nm, as shown in Fig. 1 (a) and (b). Additionally, to obtain a high-resolution (<5 μm) image close to the theoretical value, a broader full bandwidth should be detected by the spectrometer. However, detection of the broad full bandwidth results in a low depth range as shown in Eq. (2). At 840 nm, the limitation of the depth range originating from the broad full bandwidth detection can be overcome because a camera with a large pixel number above 2048 pixels is readily available. However, at 1.3 μm, it is difficult to obtain the large depth range while maintaining the theoretical axial resolution because the commercialized InGaAs line-scan camera has a maximum of 1024 pixels.

III. EXPERIMENTAL SETUP

Fig. 2 shows a schematic of our SD-OCT system. We use the SLD with a center wavelength of 1310 nm, an FWHM of 170 nm, and power of 26.5 mW (DenseLight Semiconductors Inc., Singapore), which can produce the theoretical axial resolution of 4.4 μm in air. The light from the SLD, coupled with an optical circulator and an optical coupler (10:90), is split into the sample (90 %) and reference (10 %) arms. Light reflected from the sample and reference arms is recombined and directed into a spectrometer, which is composed of a

transmission diffraction grating, an achromatic doublet lens, and an InGaAs line-scan camera.

The groove density of the grating (Wasatch Photonics, USA) is 1145 lines/mm with an incident angle of 48°. The dispersed light beam is focused via the achromatic doublet lens onto the InGaAs line-scan camera (Sensors Unlimited Inc., USA) that has 1024 pixels with 25 μm (horizontal) × 500 μm (vertical) pitch at the time clock of 12.5-MHz. To acquire a single line data (*i.e.*, data of 1024 pixels), the camera requires a minimum of 266 clocks; therefore, the maximum line rate of the camera is 46.99 klines/s (*line rate = operating clock frequency/ number of clocks*). Spectral data from the camera are digitized by a frame grabber (PCIe 1427, National Instruments Inc., USA) with a resolution of 14 bits. In the sample arm, a 2-D galvanometer (Cambridge Technology, USA) is controlled by an analog output board (PCI 6711, National Instruments Inc., USA) to obtain 2-D and 3-D images.

In SD-OCT, interference signals in the spectral domain have to be sampled as a function of the wavenumber ($k = 2\pi/\lambda$). However, in reality, interference signals are sampled as a function of the wavelength. Therefore, zero-padding interpolation, cubic spline interpolation, or linear interpolation has to be used to rescale them into the linearly sampled k-domain [13,21,22]. To reduce the calculation time, we chose the linear interpolation method. The resampled interferogram was inversely discrete-Fourier-transformed (IDFT). We developed a program using Visual C 6.0 to control both the analog output board and the frame grabber.

IV. RESULTS

1. PSF of the axial resolution in time domain vs. spectral domain

We compared the axial resolution obtained from the PSF in TD-OCT with that in SD-OCT. In the TD-OCT image, the δz is determined by the number of sampling points in a single A-scan; thus, smaller δz can be obtained by increasing the number of sampling points. Fig. 3 (a) and (b) show the PSFs in the axial direction in TD-OCT and SD-OCT, respectively, when a mirror was used as a sample with the same optical source. To obtain the axial resolution in TD-OCT, we used a separate fiber-based OCT system. For axial scanning, we used the rapid scanning delay line (RSOD) composed of a grating, a lens, a mirror, and a galvanometer [14]. While the galvanometer was driven at 1 kHz with a depth range of 1.7 mm, the Doppler frequency (f_D) was 250 kHz. We sampled the interference signals at a frequency equal to twenty times the Doppler frequency before the demodulation process. After the digital Hilbert transform, the number of axial data points was 5,000, and the δz was 0.34 μm. The measured axial resolution was 5.03 μm, as shown in Fig. 3 (a). This value is slightly larger than that of the theoretical value mainly because of the dispersion mismatch between the reference and the sample arms.

In SD-OCT, the pixel interval δz is limited by the full spectral bandwidth detected by the camera, as shown in Eq. (3). When we used the achromatic doublet lens with a focal length of 75 mm in the spectrometer, the camera detected the full spectral bandwidth of 201 nm corresponding to the depth range of 2.0 mm. Therefore, the δz was 3.9 μm. Fig. 3 (b) shows the measured axial resolution from the PSF in SD-OCT. In this figure, the axial resolution was 8.2 μm, which was significantly broadened from the theoretical axial resolution. The main sources of this broadening may be the large δz.

2. Axial resolution and Depth range

The full spectral bandwidth collected by the detector is determined by the focal length (f) of the achromatic doublet lens in the spectrometer. As the focal length of the achromatic doublet lens becomes shorter, the horizontally collimated beam size becomes smaller;

therefore, the camera can cover a broader spectrum, which exerts influence on the depth range of SD-OCT images. It can be summarized by the grating equation and the geometric optics as follows:

$$\lambda_{full}=2d \sin\left[\tan^{-1}\left(\frac{PN}{2f}\right)\right]\cos\theta_0, \quad (5)$$

where P and N are the pitch size and the total pixel number of the camera, respectively. In addition, d is the groove spacing (mm per groove) of the grating. θ_0 is the constant value 8 with 48.6°, which is the diffraction angle for the center wavelength (1310 nm) as shown in Fig. 2. Fig. 4 shows the axial resolution based on the full spectral bandwidth when the real focal length of the achromatic doublet lens is (a) 95 mm, (b) 70 mm, (c) 55 mm, and (d) 35 mm. Then, the actual depth ranges are 2.9 mm, 2.0 mm, 1.7 mm, and 1.1 mm, respectively, calculated after linear interpolation and IDFT. The full spectral bandwidths captured by the detector array were 150 nm, 214 nm, 258 nm, and 401 nm, respectively.

The δz in Fig. 4 (a), (b), and (c) were 5.7 μm, 3.9 μm, and 3.3 μm, respectively. These values are greater than half the theoretical axial resolution. Therefore, we can see the broadened axial resolution. In addition, relatively large side robes appeared in the case of (a) and (b), which are caused by the non-Gaussian spectral shape and the sharply cut boundary from the original full spectral bandwidth (approximately 250 nm) of the SLD.

On the other hand, the δz in Fig. 4 (d) was 2.1 m, which is less than half the theoretical axial resolution, thus satisfying the Nyquist sampling theorem. The measured axial resolution was approximately 5.0 μm, which is close to the theoretical value. In Fig. 4 (d), although the measured axial resolution was close to the theoretical value, the measured axial resolution was slightly larger because the PSF had a small number of sampling points. To increase the number of data points and to smooth the PSF, we used the zero-filling method to adjust the number of arbitrary data points at both edges of the spectrum before IDFT [19]. The actual number of interference signal points was 1024, and we zero-filled the data so that the total number of data points was 2048, 4096, 8192, or 16384. In this way, a smaller pixel interval can be obtained without changing the overall depth range. Fig. 5 shows the measured axial resolutions obtained by increasing the image pixel number after IDFT. The x-axis is represented by half the total pixel numbers (N) because only half of the total depth after IDFT contributes to the real image. We can see that as the number of data points is increased, the axial resolution is improved gradually. Fig. 6 shows the PSF when the number of data points at the axial direction of the SD-OCT image is 2048 after IDFT. The measured axial resolution from the PSF is very close to the theoretical value.

3. Sensitivity roll-off

The image depth range (or detected full spectral bandwidth) of SD-OCT also affects the sensitivity roll-off with depth. The sensitivity roll-off due to the depth-dependent signal drop is an important technical weakness of SD-OCT. The depth-dependent signal drop is generated by optical resolution limits of the spectrometer, finite pixel width, aliasing at high spatial frequencies, and inter-pixel cross-talk in the spectrometer [23–25]. In particular, aliasing or reduced fringe visibility at high-spatial frequencies is a major effect of the sensitivity roll-off [12]. Additionally, the rectangular shape of the camera pixels and Gaussian beam profile (Gaussian function) are convolved with the interference signal [12,24]. Therefore, the roll-off rate, R, after the Fourier transform of the interference signal is a function of the product of a sinc function and the Gaussian function as follows [12]:

$$R(z)=\left(\frac{\sin\zeta}{\zeta}\right)^2 \exp\left[-\frac{w^2}{2\ln 2}\zeta^2\right], \quad (6)$$

where $\zeta = (\pi/2)\cdot(z/z_{max})$, which is a function of the axial location normalized to the maximum depth range. Also, $w = \Delta\lambda/\delta\lambda$, where $\Delta\lambda$ is the spectrometer's spectral resolution. Therefore, changes in the depth range controlled by the detected full spectral bandwidth in the spectrometer induce changes on the sensitivity roll-off. As shown in Eq. (4), the signal roll-off rate, R, is a function of the normalized depth (z/z_{max}). Therefore, if we compare the sensitivity in the same depth position, it is clear that the sensitivity for a longer imaging depth range is higher than that for a shorter imaging depth range. Fig. 7 shows the experimental results of the sensitivity roll-off according to various full spectral bandwidths (or imaging depth ranges). When λ_{full} is 150 nm, 214 nm, and 258 nm, the sensitivity roll-off is similar up to approximately 1.0 mm depth from the surface. We found that the sensitivity for λ_{full} = 150 nm was the highest at a depth of more than 1.0 mm. We also observed a fast decay in the sensitivity as a function of the depth when λ_{full} is 401 nm, which created an imaging depth range of 1.1 mm as shown in Fig. 7 (green line).

4. SD-OCT Images

We obtained and compared several SD-OCT images for various spectral full bandwidths. The data sizes were fixed as 768 (lateral) × 1024 (axial) pixels, and the acquisition time was 16.4 ms corresponding to a frame rate of 61 fps. Currently, our system displays the OCT image with real-time of 12 fps on the monitor because of the computational burden due to linear interpolation and IDFT without the zero-filling method. Fig. 8 shows *in-vivo* images of the anterior chamber of a mouse eye. We resized each image of 768 (lateral) × 512 (axial) pixels to actual dimensions so that we could directly compare the image quality. As shown in Fig. 8 (a), we could observe the cornea, iris, and lens of the mouse in deeper areas clearly because of the long image depth range and the slow sensitivity roll-off. As expected, the overall depth range shown in Figs. 8(b) and (c) are limited. Theoretically, the image resolution improves when a larger band is used for image construction, which is not readily observable in these figures.

Fig. 9 shows *in-vivo* images of human skin on the palm. Similarly, we resized the images after obtaining images with 512 (lateral) × 512 (axial) pixels. The acquisition time was 10.9 ms (91 fps), and the display speed was 17 fps real-time. Similar to the images shown in Fig. 8, the penetration depth of the image is deeper in Fig. 9 (a) than in Figs. 9(b) and (c) due to the slow sensitivity roll-off. However, the interface between the epidermis and the dermis in Fig. 9 (c) is the clearest due to the higher axial resolution.

V. DISCUSSION

The axial resolution, imaging depth range, and sensitivity are important parameters in all OCT systems. The axial resolution depends on the center wavelength, spectral shape, and the FWHM of the optical source. A depth range of 1.5 mm ~ 3.0 mm is needed especially when 3-D volume images of the biological tissues with a large curvature are obtained as shown in Fig. 8 [26]. A high sensitivity guarantees deeper penetration depth in OCT images. Sensitivity is determined by several parameters such as optical power, scan speed, and the efficiency of the detector. Higher optical power can improve the image quality with deeper penetration depth in both TD-OCT and FD-OCT systems because higher power increases the sensitivity. In SD-OCT, the sensitivity also depends on the finite resolution of the spectrometer as well as the optical power.

It is well known that the wavelength at 1.3 μm has advantages over 800 nm in terms of the penetration depth into scattering media such as biological tissues. SD-OCT at 800-nm regions can produce a high axial resolution, a long image depth range, and slow sensitivity roll-off because line-scan cameras with larger pixel numbers have already been commercialized. On the other hand, use of the InGaAs line-scan camera for SD-OCT at 1.3-μm regions is limited because the camera with maximum pixel number of 1024 pixels is a state-of-the art product that has been just put on the market. From this study, it is clear that SD-OCT at 1.3-μm cannot satisfy the conditions both below the axial resolution of 5 μm and above the depth range of 2 mm. If a camera with a large pixel number (above 2048) is developed and commercialized, these limitations can be overcome.

To maintain a reasonable depth scan range of 2.0 mm, we chose the full spectral bandwidth of 214 nm to balance the axial resolution (8.2 μm). In this setting, the sensitivity of the system, which was determined by adding the sample attenuation constant (46.1 dB), was approximately 107.1 dB near zero optical delay when the camera was set at an exposure time of 16.96 μs. The theoretical sensitivity was approximately 120.7 dB because the efficiency of the spectrometer was ideally 63 % and the power at the sample arm was 17 mW. The sensitivity of our system was lower than that of the theoretical value mainly due to the insertion loss (−11.5 dB) between the fiber optics and the 2-D scan head in the sample arm. Additionally, losses at other optical parts reduced the sensitivity by −2.1 dB. It is our conclusion that a continuous light source with full bandwidth larger than 214 nm is not needed for a detector array of 1024 pixels if a full depth range of more than 2 mm is needed.

Currently, our system employs single-thread processing in the acquisition and display program. Although the acquisition time is fast enough to obtain an image with 512 (lateral) × 512 (axial) pixels (91 fps), the real-time display speed is limited to 17 fps because of the computation time for linear interpolation and IDFT. If we use a multi-thread programming method or a signal processing board such as a field-programmable gate array (FPGA) or a digital signal processor (DSP), the real-time display speed can be significantly improved [27–29]. Additionally, constructing a linear k-domain spectrometer to use a prism can achieve a high-speed display rate [30].

VI. CONCLUSION

In this study, we compared axial resolutions from point spread functions (PSFs) and depth ranges while changing the full spectral bandwidth detected by the camera with same optical source and describing the optimization process for the axial resolution, the depth range, and the sensitivity for our SD-OCT system. Our SLD had a center wavelength of 1310 nm and an FWHM of 170 nm corresponding to the theoretical axial resolution of 4.4 μm in air. We used a high-speed InGaAs line-scan camera (1024 pixels, 46.99 klines/s) because of its high acquisition speed. When we obtained the axial resolution from PSFs according to the detected full spectral bandwidth in the spectrometer, we found that SD-OCT at 1.3 μm cannot satisfy the conditions both below the axial resolution of 5 μm and above the depth range of 2 mm because of the restricted pixel number of the line-scan camera. When the depth range was increased, the measured axial resolution became larger than the theoretical axial resolution. On the other hand, if the axial resolution was preserved to be close to the theoretical axial resolution, the depth range and sensitivity were insufficient for OCT in turbid samples. Therefore, when the depth range was 2.0 mm, we could measure the axial resolution of 8.2 μm. In the case of SD-OCT, a sensitivity of up to 107.1 dB was achieved.

Acknowledgments

This research was supported by a grant (2009K001280) from the Brain Research Center of the 21st Century Frontier Research Program and a grant (20090090250) from Basic Research Program through the National Research Foundation of Korea (NRF) funded by the Ministry of Education, Science and Technology, Republic of Korea. This work was also supported by the research grants from the National Institute of Health (EB-00293, CA-91717, CA-124967, and RR-01192), the Air Force Office of Scientific Research (FA9550-04-1-0101), and the Beckman Laser Institute Endowment.

REFERENCES

1. Huang D, Swanson EA, Lin CP, Schuman JS, Stinson WG, Chang W, Hee MR, Flotte T, Gregory K, Puliafito CA, Fujimoto JG. Science. 1991; 254:1178. [PubMed: 1957169]
2. Kim J, Choi C, Soh K-S, Ho D-S, Kim B-M. J. Korean Phys. Soc. 2005; 47:375.
3. Kambe M, Kinoshita S, Ohmi M, Haruna M. J. Korean Phys. Soc. 2008; 53:1290.
4. Zhang J, Chen Z. Opt. Express. 2005; 13:7449. [PubMed: 19498770]
5. Fercher AF. J. Biomed. Opt. 1996; 1:157. [PubMed: 23014682]
6. Fercher AF, Drexler W, Hitzenberger CK, Lasser T. Rep. Prog. Phys. 2003; 66:239.
7. Ko TH, Adler DC, Fujimoto JG, Mamedov D, Prokhorov V, Shidlovski V, Yakubovich S. Opt. Express. 2004; 12:2112. [PubMed: 19475046]
8. Wojtkowski M, Srinivasan VJ, Ko TH, Fujimoto JG, Kowalczyk A, Duker JS. Opt. Express. 2004; 12:2404. [PubMed: 19475077]
9. Leitgeb RA, Drexler W, Unterhuber A, Hermann B, Bajraszewski T, Le T, Stingl A, Fercher AF. Opt. Express. 2004; 12:2156. [PubMed: 19475051]
10. Herz PR, Chen Y, Aguirre AD, Fujimoto JG, Mashimo H, Schmitt J, Koski A, Goodnow J, Petersen C. Opt. Express. 2004; 12:3532. [PubMed: 19483882]
11. Tumlinson AR, Povazay B, Hariri LP, McNally J, Unterhuber A, Hermann B, Sattmann H, Drexler W, Barton JK. J. Biomed. Opt. 2006; 11 064003.
12. Yun SH, Tearney GJ, Bouma BE, Park BH, de Boer JF. Opt. Express. 2003; 11:3598. [PubMed: 19471496]
13. Yasuno Y, Madjarova VD, Makita S, Akiba M, Morosawa A, Chong C, Sakai T, Chan KP, Itoh M, Yatagai T. Opt. Express. 2005; 13:10652. [PubMed: 19503280]
14. Rollins AM, Kulkarni MD, Yazdanfar S, Ungarunyawee R, Izatt JA. Opt. Express. 1998; 3:219. [PubMed: 19384364]
15. Yun SH, Tearney GJ, de Boer JF, Iftimia N, Bouma BE. Opt. Express. 2003; 11:2953. [PubMed: 19471415]
16. Hausler G, Lindner MW. J. Biomed. Opt. 1998; 3:21. [PubMed: 23015002]
17. de Boer JF, Cense B, Park BH, Pierce MC, Tearney GJ, Bouma BE. Opt. Lett. 2003; 28:2067. [PubMed: 14587817]
18. Liu B, Brezinski ME. J. Biomed. Opt. 2007; 12 044007.
19. Takahashi Y, Watanabe Y, Sato M. Appl. Opt. 2007; 46:5228. [PubMed: 17676135]
20. Takahashi Y, Watanabe Y, Sato M. Jpn. J. Appl. Phys. 2008; 47:6540.
21. Press, WH.; Teukolsky, SA.; Vetterling, WT.; Flannery, BP. Numerical Recipes in C. Cambridge University Press; 1992.
22. Dorrer C, Belabas N, Likforman J, Joffre M. J. Opt. Soc. Am. B. 2000; 17:1795.
23. Hu ZL, Pan YS, Rollins AM. Appl. Opt. 2007; 46:8499. [PubMed: 18071382]
24. Bajraszewski T, Wojtkowski M, Szkulmowski M, Szkulmowska A, Huber R, Kowalczyk A. Opt. Express. 2008; 16:4163. [PubMed: 18542513]
25. Potsaid B, Gorczynska I, Srinivasan VJ, Chen YL, Jiang J, Cable A, Fujimoto JG. Opt. Express. 2008; 16:15149. [PubMed: 18795054]
26. Bouma BE, Tearney GJ. Handbook of Optical Coherence Tomography. 2002
27. Park BH, Pierce MC, Cense B, de Boer JF. Opt. Express. 2003; 11:782. [PubMed: 19461791]
28. Su JP, Zhang J, Yu LF, Colt HG, Brenner M, Chen Z. J. Biomed. Opt. 2008; 13 030506.

29. Ustun TE, Iftimia NV, Ferguson RD, Hammer DX. Rev. Sci. Instrum. 2008; 79 024302.
30. Hu Z, Rollins AM. Opt. Lett. 2007; 32:3525. [PubMed: 18087530]

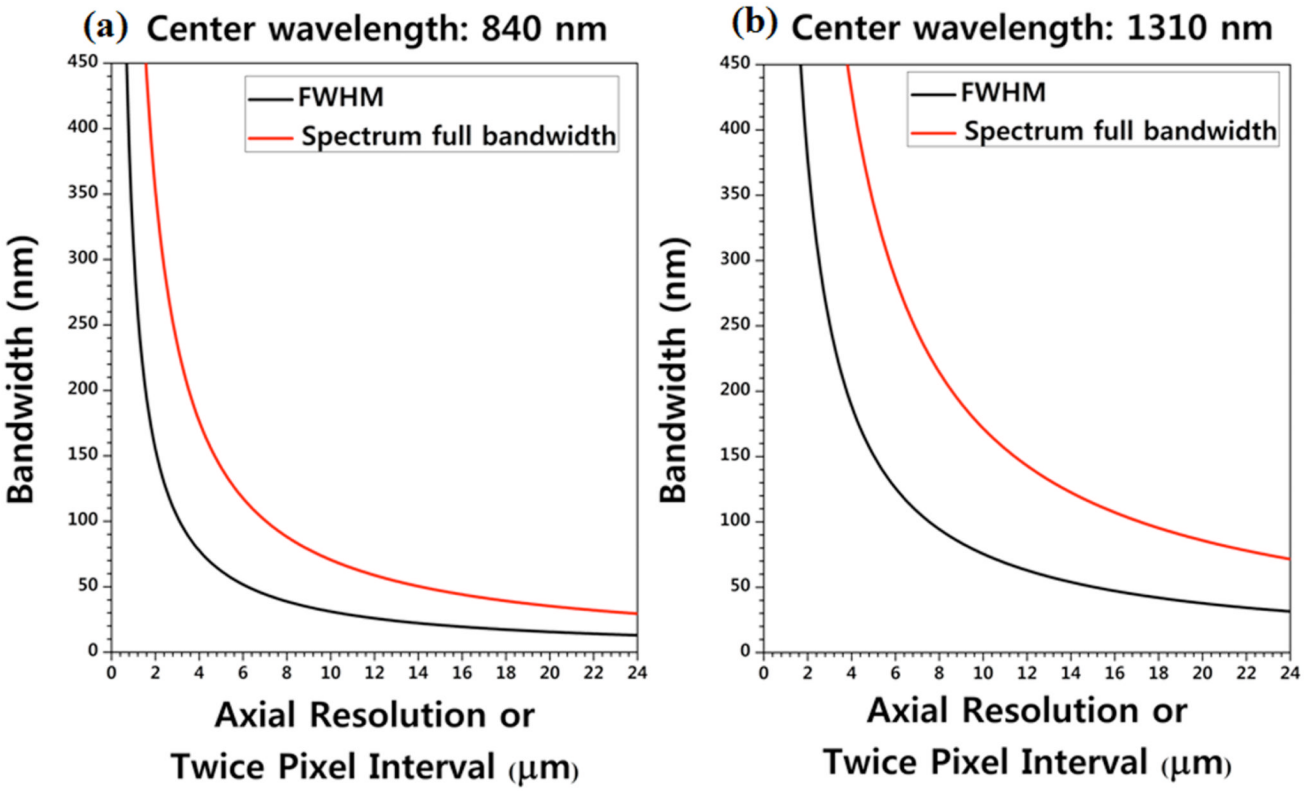

Fig. 1.
Axial resolutions calculated with the FWHM of the light source (black) and twice the interval ($2\delta z$) calculated with the spectrum full bandwidth detected by the spectrometer (red).

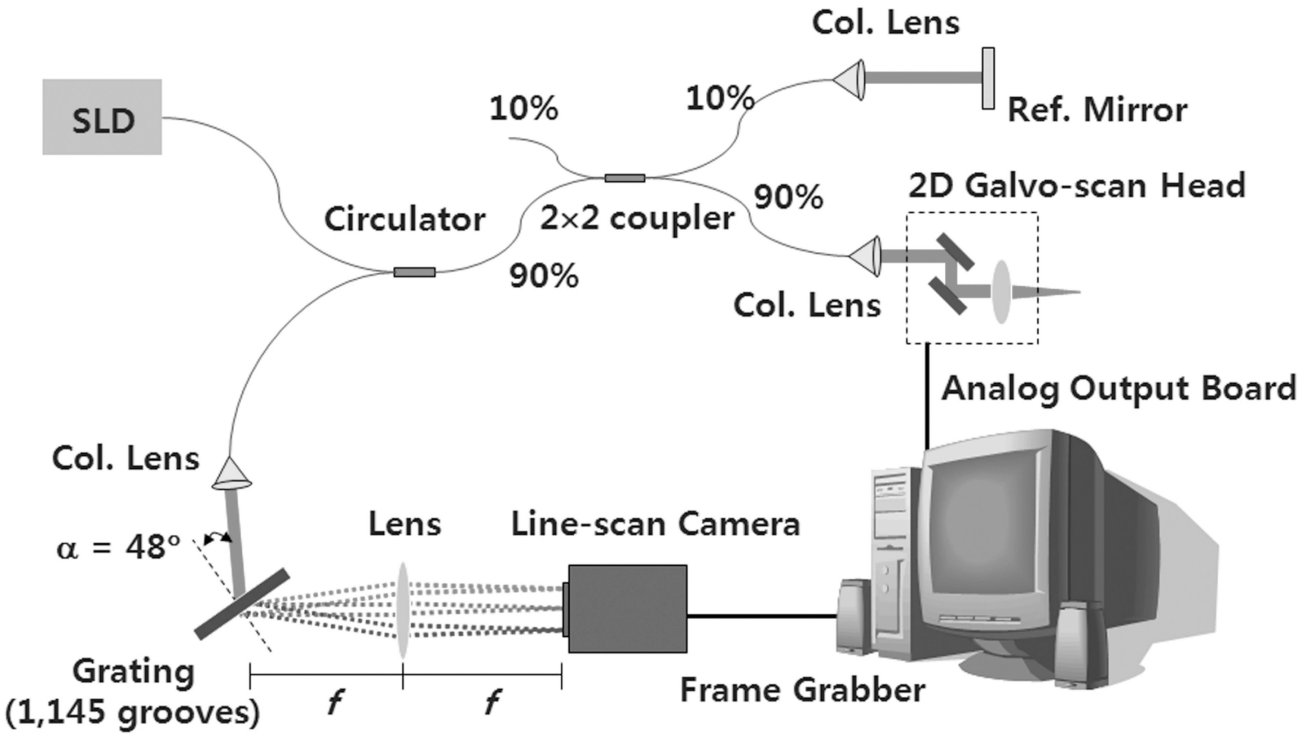

Fig. 2.
Schematic of our spectral-domain OCT system.

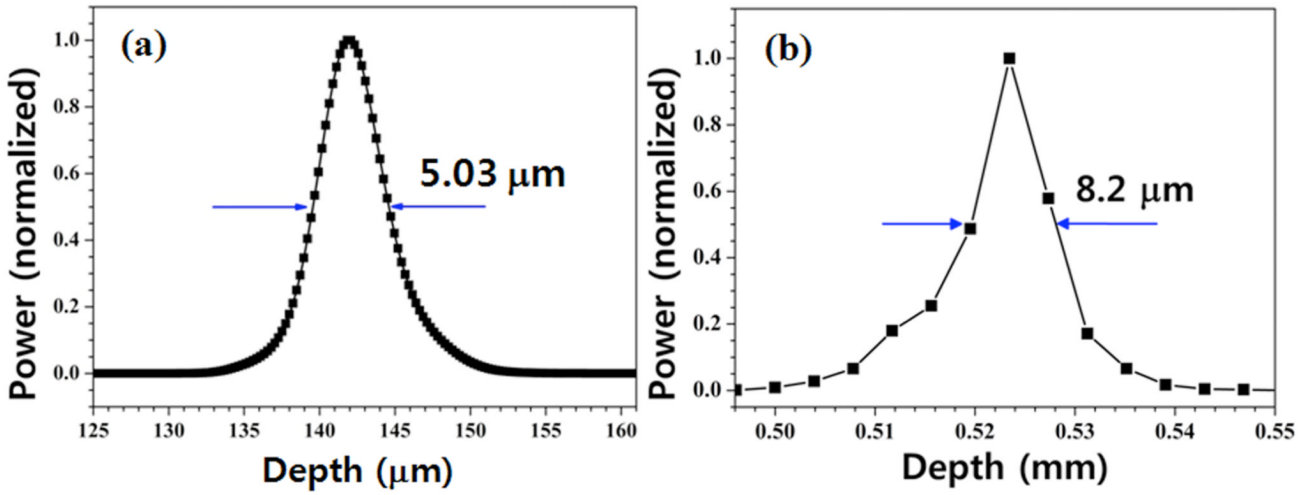

Fig. 3.

Point spread function of the axial resolution when the SLD has a center wavelength of 1310 nm and an FWHM of 170 nm. (a) Time domain system, (b) Spectral domain system. The data points in the time domain and spectral domain systems are 5000 points/line and 512 points/line, respectively.

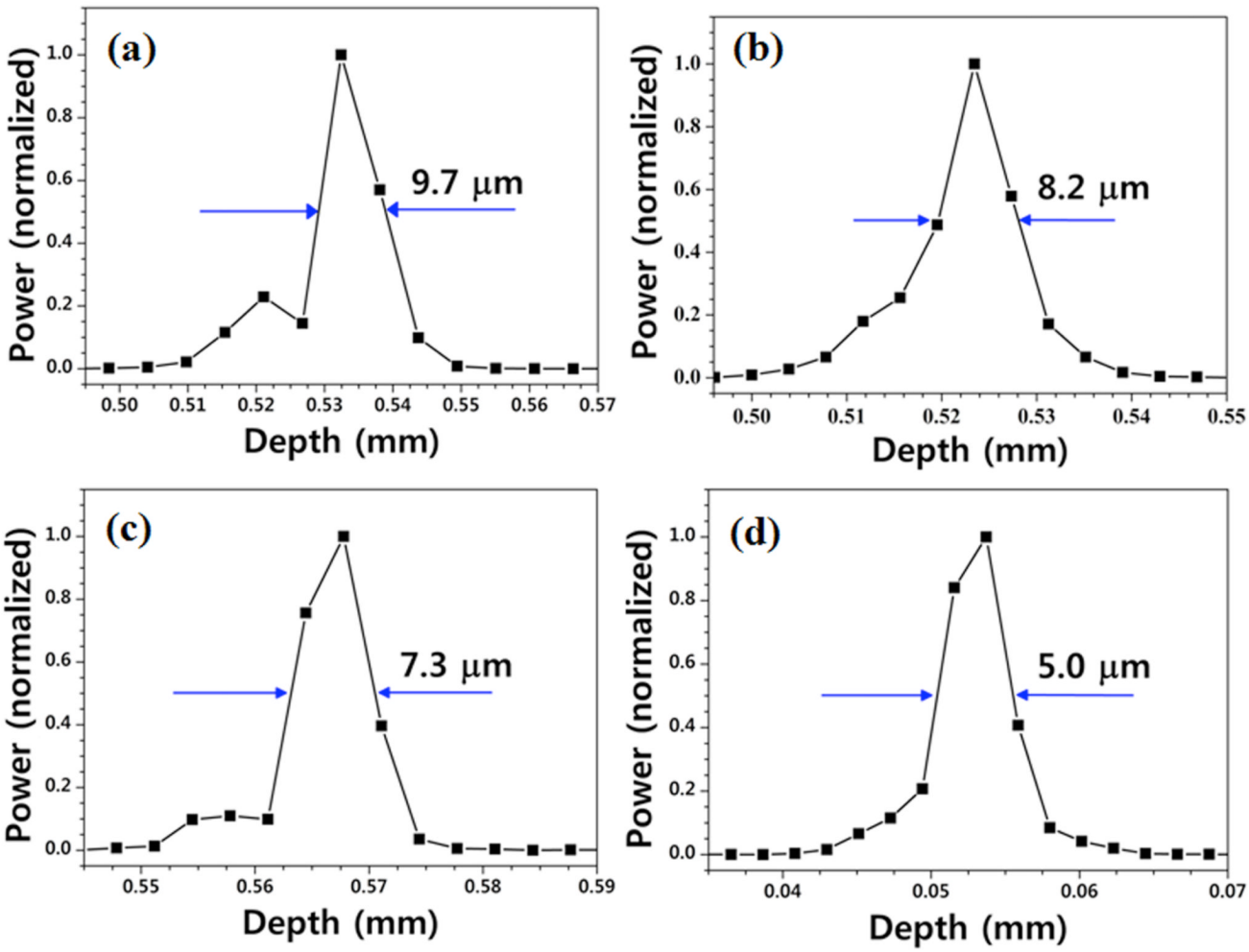

Fig. 4.

Point spread function of the axial resolution according to the spectrum full bandwidth the spectrometer detected when the SLD has a center wavelength of 1310 nm and an FWHM of 170 nm. (a) f = 95 mm (λ_{full} = 150 nm, z_{max} = 2.9 mm), (b) f = 70 mm (λ_{full} = 214 nm, z_{max} = 2.0 mm), (c) f = 55 mm (λ_{full} = 258 nm, z_{max} = 1.7 mm) and (d) f = 35 mm (λ_{full} = 401 nm, z_{max} = 1.1 mm). The data points are 512 points/line.

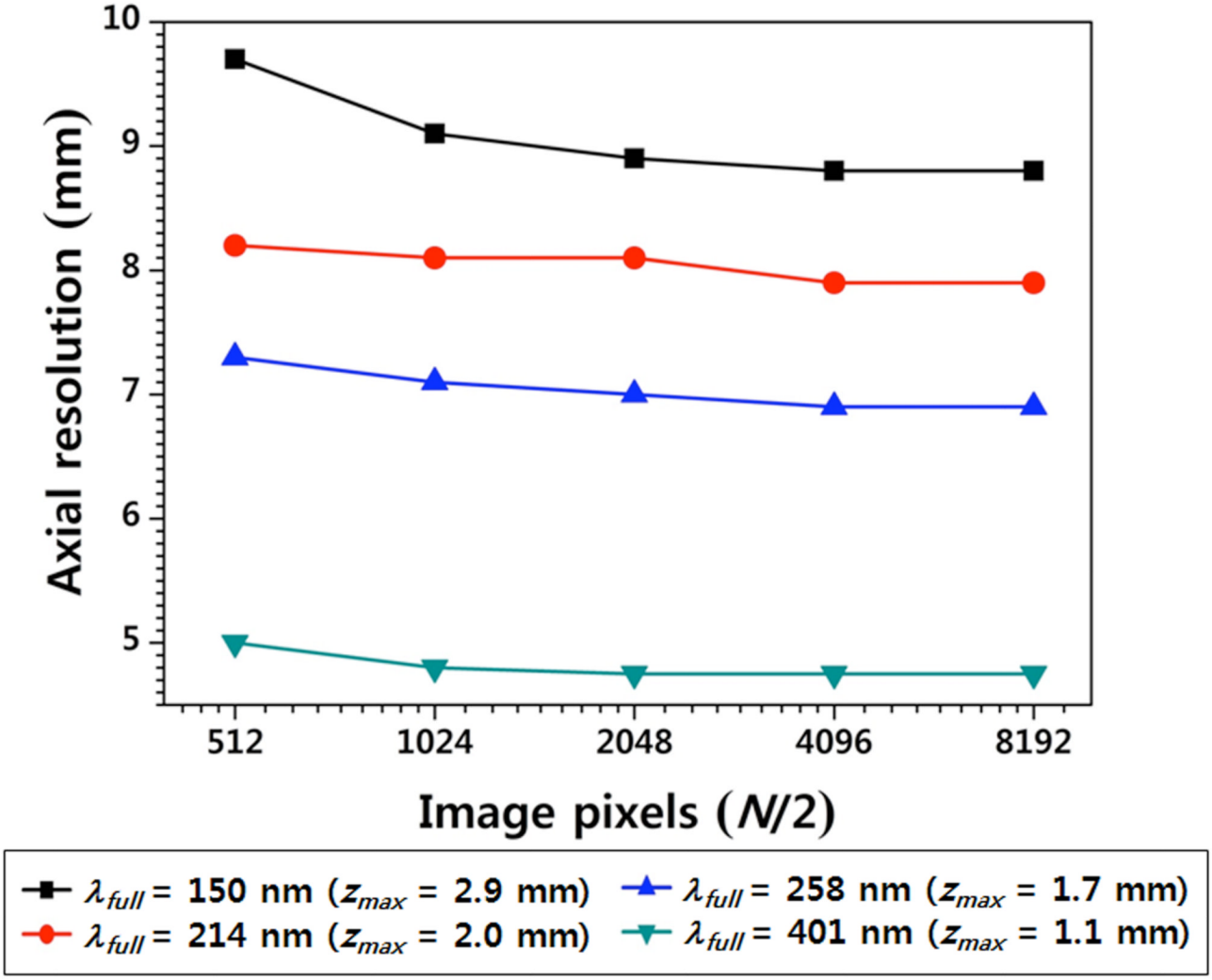

Fig. 5.
Enhanced axial resolution according to image pixel number after zero-filling and inverse discrete Fourier transforming when we used the mirror as the sample. *N* is the total number of data points.

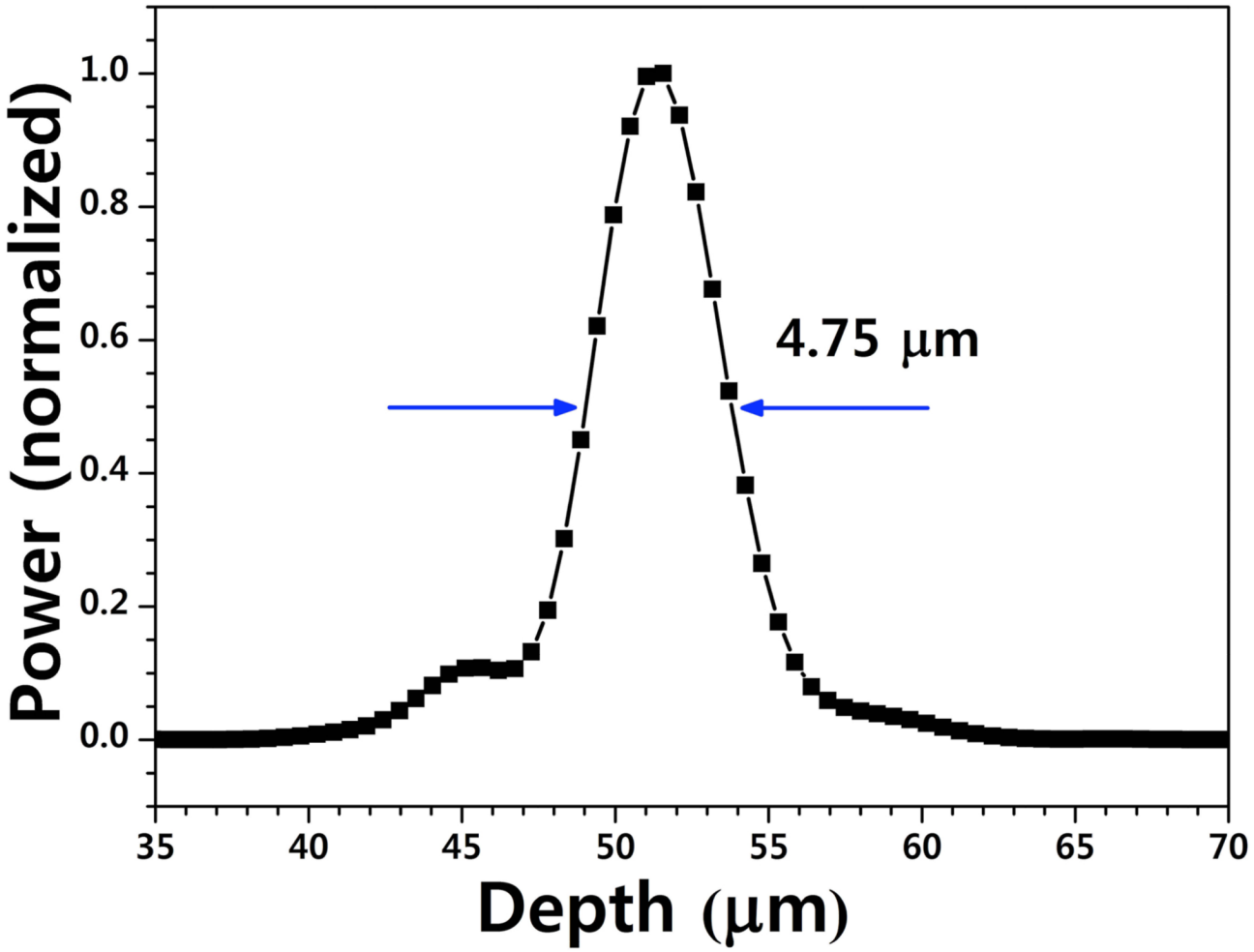

Fig. 6.
Enhanced the point spread function of the axial resolution after zero-filling when the SLD with a center wavelength of 1310 nm and an FWHM of 170 nm.

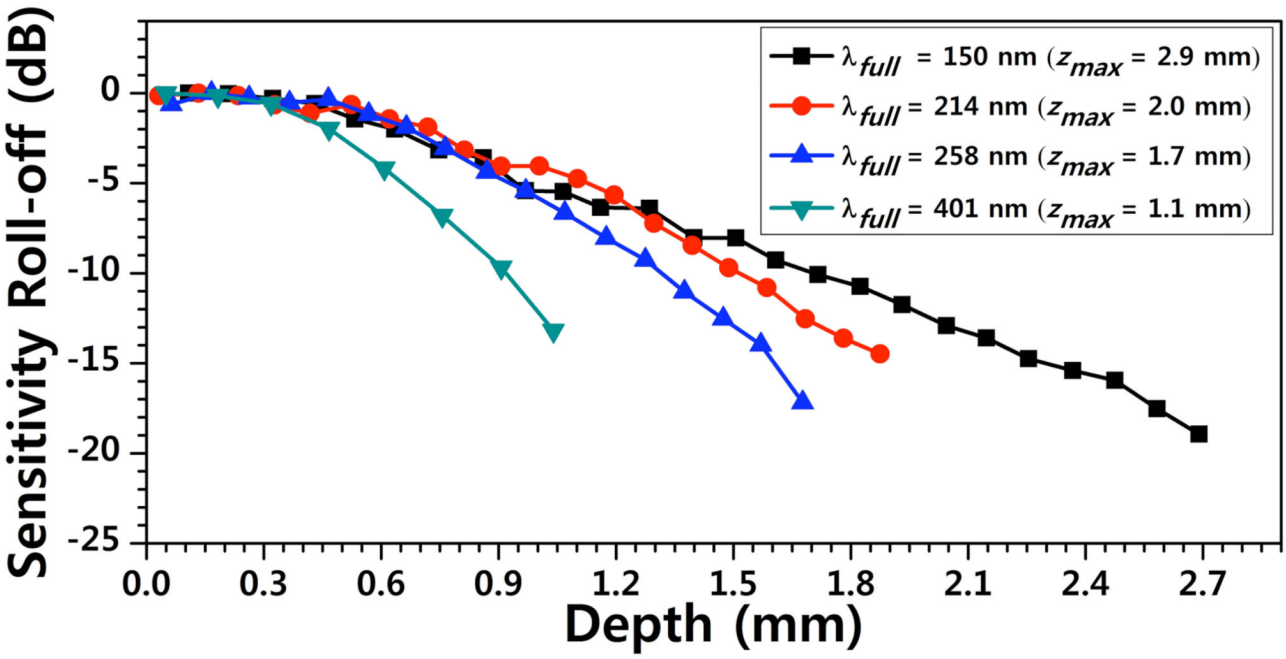

Fig. 7.
Sensitivity roll-off according to the spectrum full bandwidth (imaging depth range).

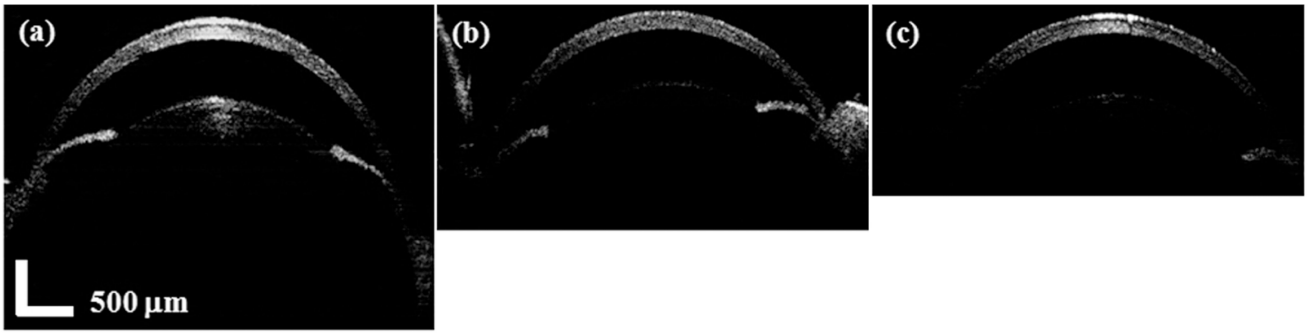

Fig. 8.

In-vivo images of the anterior chamber of the mouse eye according to the spectrum full bandwidth obtained by using various achromatic lenses with focal lengths: (a) f = 95 mm (λ_{full} = 150 nm, z_{max} = 2.9 mm), (b) f = 70 mm (λ_{full} = 214 nm, z_{max} = 2.0 mm) and (c) f = 55 mm (λ_{full} = 258 nm, z_{max} = 1.7 mm). Each image was resized after the image was obtained with 512 (axial) × 768 (lateral) pixels. The lateral physical size is approximately 3.8 mm.

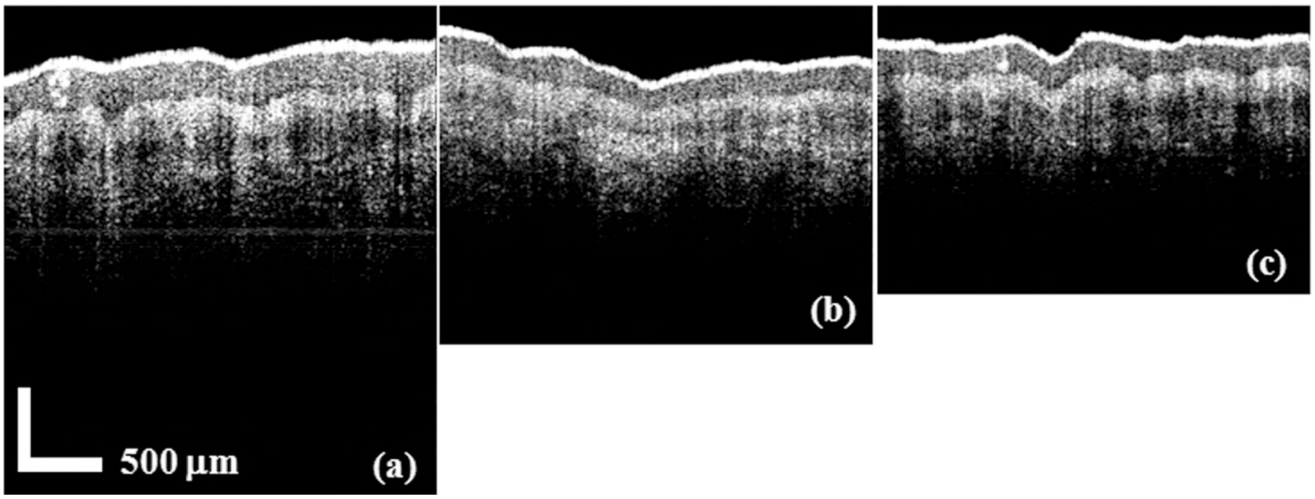

Fig. 9.

In-vivo images of the human skin in a palm according to the spectrum full bandwidth: (a) f = 95 mm (λ_{full} = 150 nm, z_{max} = 2.9 mm), (b) f = 70 mm (λ_{full} = 214 nm, z_{max} = 2.0 mm), and (c) f = 55 mm (λ_{full} = 258 nm, z_{max} = 1.7 mm). Each image was resized after the image was obtained with 512 (axial) × 512 (lateral) pixels. The lateral physical size is approximately 2.5 mm.